The geometrical characteristics of fcc, hcp, and polycrystalline nanowires: simulations of transmission electron microscopy images and diffraction patterns

J.M. Montejano-Carrizales[a], R.A. Guirado-López[a], J.L. Rodríguez-López[b], and J.L. Morán-López[b,c]
[a]*Instituto de Física, Universidad Autónoma de San Luis Potosí, Álvaro Obregón 64, 78000 San Luis Potosí, S.L.P., Mexico.*
[b]*División de Materiales Avanzados Instituto Potosino de Investigación Científica y Tecnológica, A.C., San Luis Potosí, México.*
[c]*División de Ingeniería y Ciencias, Universidad Politécnica de San Luis Potosí, Urbano Villalón 500, 78369 San Luis Potosí, S.L.P., Mexico.*

Recibido el 25 de febrero de 2009; aceptado el 02 de junio de 2009

To theoretically study the physicochemical properties of nanowires, it is necessary to build the corresponding atomic geometrical models. Here we present the geometrical characteristics of nanowires with fcc, hcp, and polycrystalline structures. We consider fcc and hcp wires grown along the (111) and z axis directions, respectively, with various diameters and lengths. In addition, since staking faults in these systems are very common, we analyze also the case of nanowires formed by stacked pieces having different crystalline structures and orientations, a fact that leads to the formation of several internal interfaces. By performing simulations of transmission electron microscopy (TEM) images and diffraction patterns of the nanowires considered here, we reveal how sensitive are the calculated images to the defocus condition as well as to the orientation of the wire with respect to the incident beam, a result that must be taken into account in order to better understand the measured data.

Keywords: Nanowires; fcc nanostructures; hcp nanostructures; TEM simulations; diffraction patterns.

Para el estudio teórico de las propiedades fisico-químicas de alambres es necesario construir el correspondiente modelo geométrico. Presentamos las caracteríisticas geométricas de nanoalambres con estructuras fcc, hcp y policristalinos. Consideramos alambres fcc y hcp crecidos a lo largo de las direcciones (111) eje z respectivamente, con varios diámetros y longitudes. Ademaś, como en estos sistemas son comunes las fallas de crecimiento (stacking faults), también analizamos el caso de nanoalambres formados por tramos que tienen diferentes estructuras cristalinas y orientaciones, lo que lleva a la formación de varias interfases internas. Llevando a cabo la simulacion de imágenes de alta resolución en microscopía de transmisión de electrones (TEM) y de sus respectivos patrones de difracción de los nanoalambres aquí considerados, hacemos notar lo sensitivas que son a las condiciones de enfoque las imágenes calculadas, así como también a la orientación de los nanoalambres con respecto al haz incidente, un resultado que debe tenerse en cuenta para un mejor entendimiento de las mediciones obtenidas.

Descriptores: Nanoalambres; nanoestructuras fcc; nanoestructuras hcp; simulaciones TEM; patrones de difracción.

PACS: 81.07.Dc; 75.75.+a; 36.40.Cg

1. Introduction

Due to the effects of spatial confinement and low dimensionality, nanostructures exhibit physicochemical properties not displayed by the corresponding bulk solids. Particularly unique properties of nanowires, and related one dimensional nanostructures, hold outstanding promise for numerous technological uses ranging from semiconductor nanomanufacturing to a variety of advanced electronic, opto-electronic, environmental, and biomedical devices [1]. In addition, careful measurements of the magnetic properties of small magnetic aggregates, nanowire arrays, and single molecule magnets, published in the last decade, show that low dimensional systems posses enhanced magnetic properties [2].

These features make nanometric systems very important, since they may lead to the development of new devices in magnetic storage media with a huge density capacity. For example, in this emerging field of spin electronics in data storage, magnetic nanowires are the essential parts for a new class of non-volatile-storage memories. In addition, ordered arrays of magnetic nanostructures are extremely interesting to study since one can investigate individual as well as the collective behavior of the constituents in a well-defined and reproducible fashion.

However, to make these applications a reality, it is necessary to grow or ensemble in a controlled manner, monodisperse periodic systems. In this sense, arrays of clusters or nanowires are some of the most promising systems. It has been observed that arrays of magnetic nanowires show enhanced coercivities that suggest applications in ultra high density magnetic storage [2–4]. Martin *et al*. [2] emphasize that due to recent advances in experimental techniques to grow ordered nanowire arrays, nowadays one can synthesize, characterize, and design special materials with specific size, composition, structure, and interwire distance.

In recent years, two interesting ways to synthesize magnetic nanowire arrays have been reported. One is to fill a porous mask with bundles of carbon nanotubes containing magnetic materials [5, 6]. The other proposal is to fill directly nanoporous templates, with a well defined pore geometry [4], with magnetic materials. The advantage of the first technique is that carbon nanotubes shield the magnetic material from oxidation, but the drawback is that it is not yet possible to control the growth of C-nanotubes with the same structure,

diameter and length. Although some advances in growing single crystals of single-walled C-nanotubes using thermolysis of nano-patterned precursors have been reported, still some problems have to be solved [5]. For example, the carbon nanotubes do not have all the same amount of magnetic material.

On the other hand, magnetic nanowires grown directly over ultrahigh-density arrays of nanopores with high aspect ratio using the equilibrium self-assembled morphology of asymmetric diblock copolymers have been produced, but they may be exposed to oxidation when the mask is removed. As a consequence, this may lead to a modification of the magnetic properties of the system [7].

From the theoretical point of view, it is clear that to carry any study of the physicochemical properties of nanowires it is necessary to model them and assume a given crystalline structure, diameter, and length, *i.e.* to know the spatial coordinates of the atoms forming the system [7, 8]. For example, in hard materials the direction of the magnetization is determined mainly by the direction of the magnetic anisotropy fields which are intrinsic to the material. In contrast, the magnetization direction in magnetically soft materials (Fe, Co, and Ni) is defined by the geometrical shape of the nanowire.

Being Co one of the most studied in different structures and arrays, specially nanowires from the experimental point of view [7, 9], here, we study the geometrical characteristics of Co nanowires with fcc and hcp structures and consider also the case in which a nanowire is formed by several grains with different structures and orientations. It is well known that theoretical calculations in nanoscopic systems are very computationally demanding, since the non-equivalency of the different sites in the system has to be taken into account. Therefore, one has to exploit any symmetry that may reduce the number of equations to be solved. Here, we consider as equivalent sites those that are at the same distance from an origin and that have the same local atomic environment.

With this in mind, we address recipes to build Co nanowires that could be used in model calculations for nanowires grown along different crystallographic directions and include cases with defects (twined and faulted). We give the tables that contain the information on how the number of atoms, and the non-equivalent sites depend on the lattice structure, diameter, and length of the nanowire.

In Sec. 2, we discuss the case of fcc nanowires growth along the (111) direction. Since stacking faults are easily formed in fcc systems, we also address nanowires consisting of two and three segments with fcc structure but with different relative orientations, and whose boundaries are formed with units that do not follow the fcc sequence. In Sec. 3 we analyze the case of nanowires constructed by following the hcp structure. We have defined the z-direction as the one perpendicular to the hexagonal planes. A more relevant stacking fault is addressed in Sec. 4 by considering polycrystalline nanowires made of segments with fcc and hcp structures.

We present in Sec. 5 our results for the simulation of transmission electron microscopy (TEM) images as well as of diffraction patterns. Although, the contrast in our simulated images for systems with different atomic structure is noticeable, we conclude that the structural characterization through this technique must be taken with caution and needs to be supported by additional characterization techniques. Finally, we present in Sec. 6 the summary and conclusions.

2. Nanowires with fcc structure

A nanowire may be considered as a cylindrical fragment of a solid with a given crystalline structure, a well defined diameter and height, and grown along a particular direction. Thus, to construct the nanowire we identify first the planes perpendicular to the axis that contain the atoms of the three dimensional lattice. Next, depending on the diameter we identify the units that are formed on the different kinds of planes. Finally, we add, as many units as needed to obtain the desired length. In all cases the nearest neighbor interatomic distance is set equal to 1. Under this scheme, we consider first the case of fcc structures.

2.1. (111) fcc nanowires

The fcc lattice, as grown in the (111) direction, can be described as follows; one forms a triangular lattice of atoms as the first layer of the solid. Then one puts atoms on the top in alternate interstices of the first layer to construct the second layer. To continue stacking triangular planes one has two options: one puts atoms just above the atoms in the first plane or one puts atoms above the interstices of the first plane that were not covered by those in the second plane. In the first case one obtains a hexagonal closed packed structure and in the second one builds a face centered cubic crystal. In this subsection, we consider the fcc structure; the hcp nanowires are considered in the next one.

Then, when constructing nanowires in the (111) direction, we have three kinds of planes, each one rotated 60° degrees with respect to the adjacent planes and arranged as mentioned above. We consider first the case of a nanowire formed by units made of seven atoms of the triangular lattice, and two other planes containing three atoms each, but rotated, according to the fcc geometry. The axis of the wire passes through the central atom of the seven atom arrangement. This is shown in Fig. 1a, in which we show the three units and, four short wires with 39, 45, 47, and 59 atoms. In this sequence, we show four options to end the wire, with one triangle after the hexagon, with two triangles after the hexagon, with one single atom of the hexagonal units, and with two hexagonal units. The wire diameter is 2. In Figs. 1b and 1c we display thicker wires with diameters 2.3 and 3.05, respectively. These systems contain 95 and 155 atoms, respectively.

To identify the non-equivalent sites one notices that each hexagon has two and in the triangular units all sites are equivalent. To enumerate the characteristics of these nanowires, we consider as the origin of coordinates, the center of the hexa-

TABLE I. Number of atoms N, and non-equivalent sites $N_{\rm neq}$ for a fcc wire grown in the (111) direction, consisting of two parts matched with two rotated hexagons (Fig. 3). The diameter is 2.

N	14	20	26	40	46	52	66	72	78	92	98	104	118	124	130	$\cdots$
$N_{\rm neq}$	2	3	4	6	7	8	10	11	12	14	15	16	18	19	20	$\cdots$

gon in the middle and grow the system adding one unit on both sides. In Table I we present how the number of atoms and of non-equivalent sites increase, for the three different wire diameters. The boldface numbers correspond to the examples given.

2.2. Polycrystalline structures

In order to model the stacking faults in the nanowire growth, we present four different views of a nanowire with diameter 2 and consisting of 111 atoms, corresponding to rotations along the wire axis. Figures 2a–2d represent the same nanowire rotated $0°$, $30°$, $60°$, and $90°$, respectively. Since the hexagonal planes coincide every $60°$, the Figs. 2a and 2c, and 2b and 2d show only differences in the triangular units.

Now we ensemble two pieces in which the geometry of the interface consists of two hexagons rotated by $30°$ (Fig. 3). In this case and taking the origin of coordinates in the plane just in between the two hexagons, each hexagon contains two non-equivalent sites, but they are equivalent with respect to the origin. Then when we add the next triangles on each side of the hexagons, they are all equivalent among them and add a non-equivalent site to the system. The same happens when one adds the next two triangles. After that the next pieces are hexagons with two non-equivalent sites, and so on. In Table II we present how the wire grows in total number of atoms and in non-equivalent sites.

As a last example of this kind of nanowires, we present a wire with two stacking faults (Fig. 4). The central piece is rotated $30°$ respect to the other two segments and the boundaries on each side of the central part consist of hexagons. The table of non-equivalent sites as one grows the wire can be constructed choosing the origin at the center of the middle hexagon.

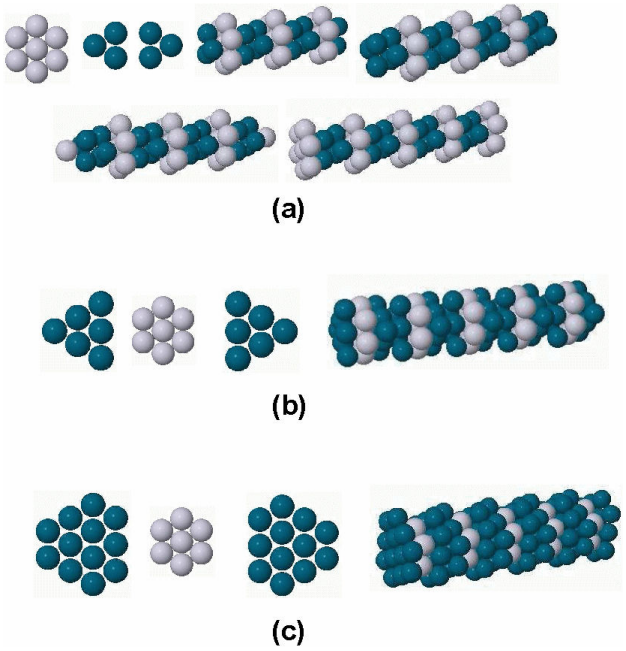

FIGURE 1. The construction of fcc-nanowires along the (111) direction with various diameters. In each figure the units perpendicular to the axis are shown, in gray the triangular lattice with central site and in blue two triangular lattices without central site rotated among them $60°$. The diameters are (a) $d = 2$, (b) $d = 2.3$, and (c) $d = 5.05$.

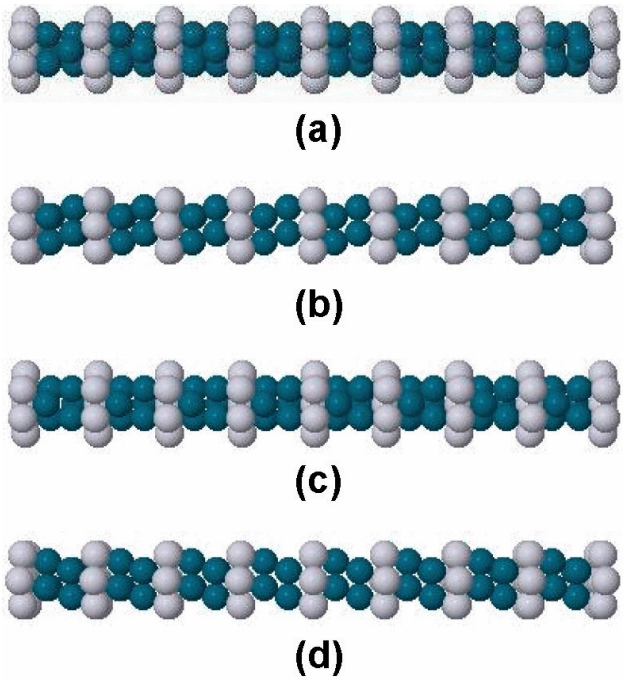

FIGURE 2. A (111) fcc-nanowire of diameter 2, rotated by (a) $0°$, (b) $30°$, (c) $60°$, and (d) $90°$. Colours as in Fig. 1.

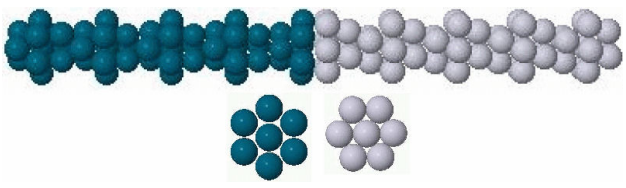

FIGURE 3. fcc-nanowires grown in the (111) direction with a stacking fault, the gray fragment is rotated $30°$ with respect to the blue one. The units at the boundary are shown. The diameters of the wires are $d = 2$.

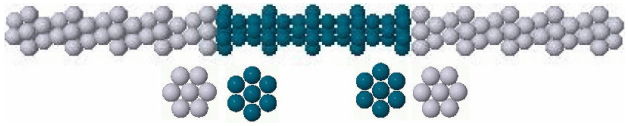

FIGURE 4. fcc-nanowires grown along the (111) direction with two stacking faults, the gray fragments are rotated 30° with respect to the blue one. The units at the boundaries are shown.

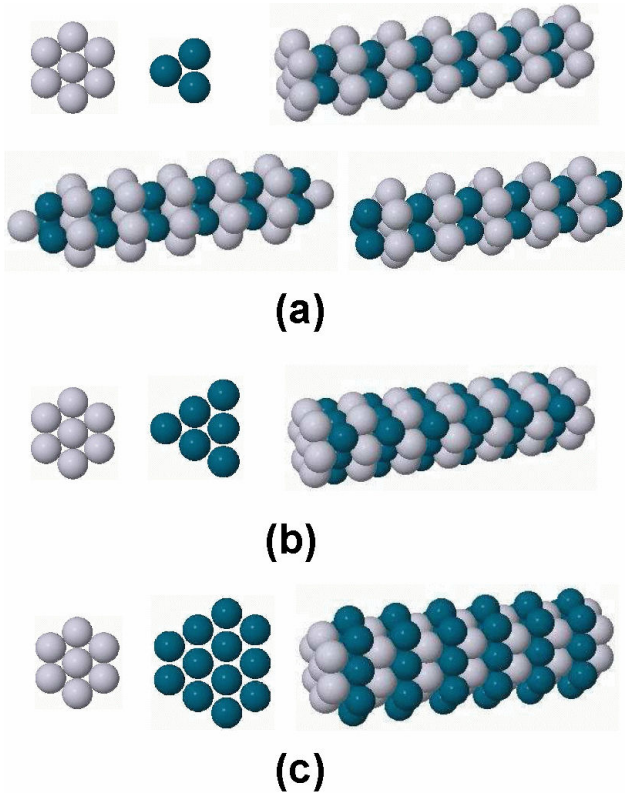

FIGURE 5. Construction of hcp-nanowires along the z-direction with various diameters. In each figure the units perpendicular to the axis are shown, in gray (blue) the triangular lattice with (without) central site. The diameters are (a) $d = 2$, (b) $d = 2.3$, and (c) $d = 5.05$.

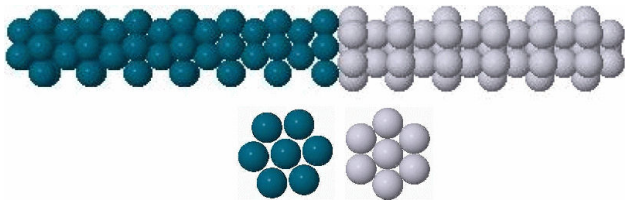

FIGURE 6. hcp-nanowires grown in the z-direction with a stacking fault, the gray fragment is rotated 30° with respect to the blue one. The units at the boundary are shown. The diameters of the wires are $d = 2$.

3. Nanowires with hcp structure

We mentioned above that the hexagonal closed packed structure consists of the staking of triangular planes, *i.e.*, taking a triangular plane, the next one is also triangular with the atoms located at the interstices of the plane below. The next triangular plane is located just above the first one, and so on. Thus, in this case there are only two types of planes.

3.1. hcp$_z$ nanowires

If we define as the z axis, the direction perpendicular to the triangular planes, one has that the planes are only of two types. If we locate the origin of coordinates in an atom, then the simplest case would be an hexagon with a central atom and the neighbor planes would consists of triangles. These two units are shown in Fig. 5a. In this figure we show similar nanowires that end with triangles, with hexagons and single atoms. Figures 5b and 5c show nanowires with larger diameters, 2.3 and 5.05, respectively. The number of atoms in these examples are 67 (the largest in Fig. 5a), 85, and 121. Similar to the fcc(111) nanowires, the hexagonal units have two non-equivalent sites and the triangles have only one. To enumerate the atoms and non-equivalent sites as one grows the wire, the origin of the central atom of the hexagon can be chosen.

3.2. Polycrystalline structures

In a similar way to the fcc nanowires, one can consider nanowires with staking faults. We show in Fig. 6 a case in which we rotate two pieces by 30° and the interface units are hexagons. Here, we show the units located at the interface. Each atom of the hexagons has two neighbors on the neighbor hexagon at a distance of 1.09 and the two central atoms are 0.96 apart. Taking the origin at the interface between the hexagons, and considering alternatively units at the right and left, the enumeration table can be constructed.

We present also the case of two staking faults. The hcp nanowire consists of three pieces rotated 30° among each other and the boundaries on each side of the central part, consist of hexagons (see Fig. 7). To build the enumeration table we chose the origin of coordinates in the middle of the two hexagons.

4. fcc(111)-hcp$_z$ nanowires

The most observed stacking faults are of the type fcc(111)-hcp$_z$, in which, as discussed above, the growing sequence of the hexagonal planes of the fcc (111) structure is interrupted. Face centered cubic structures differ from hexagonal closed packed arrays only in the stacking order: both structures have closed packed atomic planes with three-fold symmetry. When stacking one of these layers on the top of the other, the atoms are not directly on the top of one another. The first two layers are identical for both structures, and labeled, lets say AB. The difference comes in the third layer; if it is placed so that its atoms are directly above those of the first layer, the stacking will be ABA producing the hcp structure, and continues ABABAB. However, if the atoms in the third layer are not above those in the first, one produces the stacking ABC. By continuing with this process ABCABC one produces the fcc

structure. A stacking fault is produced when one of the above sequences is interrupted to follow the other one, for example the sequence ABCABCABABAB denotes that up to the six first layers the structure follows an fcc growth mode and the rest is an hcp sequence. We will denote this sequence by $(ABC)_2(AB)_3$.

We show in Fig. 8a, the fcc(111)-hcp$_z$ nanowire with the sequence $C(ABC)_4(AB)_6$. The fcc growing sequence is interrupted after four ABC-blocks. Then six blocks of the hcp structure are grown. Taking the origin at the interface between the hexagon (A unit) and the triangle (C unit), and considering alternatively units at the right and left, the enumeration table can be constructed.

Other example with a more drastic fault is shown in Fig. 8b, in which the fcc(111)-hcp$_z$ nanowire with the sequence $(BCA)_4(AB)_6$ is displayed. Here the fcc sequence is interrupted by locating an unit A (hexagon) instead of a B unit. It is important to notice that in order to fit the two hexagonal units they have to be rotated by an angle of 30° degrees. The characteristics of this nanowire can be found in a similar way that in Fig. 8a.

We consider now a wire with two stacking faults. In Fig. 9a we show a nanowire consisting of three parts; the left and right parts are fcc and the central one is hcp. The boundaries are formed by hexagons (unit A) and triangles. This wire can be denoted in two forms, because the hexagonal unit can belong to the fcc or to the hcp part, $C(ABC)_4(AB)_6ABC(ABC)_3AB$ (as in Fig. 9a) or $C(ABC)_4(AB)_6(ABC)_4AB$.

A more drastic two fault system is shown in Fig. 9b. In this case the boundary between the hcp central part and the fcc extremes consists of two hexagons. The wire can be denoted by $C(ABC)_4A(AB)_6A(ABC)_4AB$. The characteristics of these two examples can be found taking the origin at the hexagonal unit in center of the hcp wire.

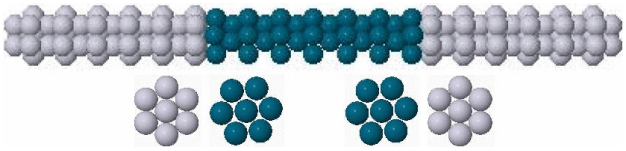

FIGURE 7. hcp-nanowires grown along the z-direction with two stacking faults, the gray fragments are rotated 30° with respect to the blue one. The units at the boundaries are shown.

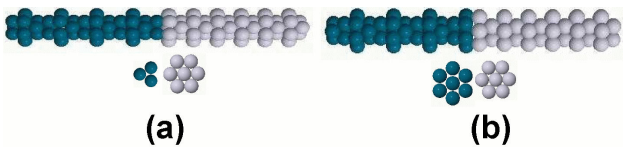

FIGURE 8. fcc(111)-hcp$_z$ nanowire with one stacking fault, in gray (blue) the hcp (fcc) fragment. The units at the boundaries are shown and consist of (a) a triangle and a hexagon and (b) two hexagons with a central atom rotated by an angle of 30°.

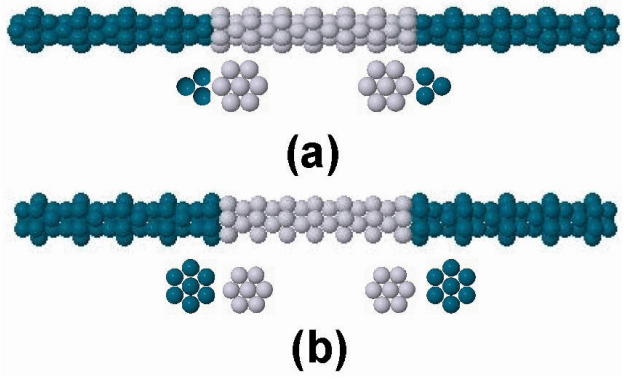

FIGURE 9. fcc(111)-hcp$_z$ nanowire with two stacking faults, in gray (blue) the hcp (fcc) fragments. The units at the boundaries are shown and consist of (a) a triangle and a hexagon and (b) two hexagons with a central atom rotated by an angle of 30°. The central part is hcp and the external sections are fcc.

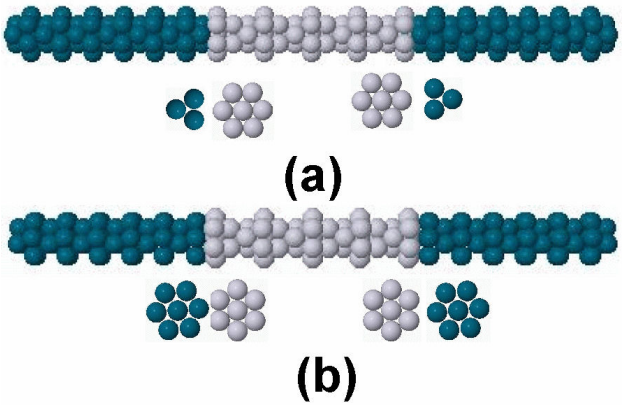

FIGURE 10. fcc(111)-hcp$_z$ nanowire with two stacking faults, in gray (blue) the hcp (fcc) fragments. The units at the boundaries are shown and consist of (a) a triangle and a hexagon and (b) two hexagons with a central atom rotated by an angle of 30°. The central part is fcc and the external sections are hcp.

Other possibility is to have a two fault nanowire in which the central part is fcc and the extremes are hcp. In Fig. 10a, we present the nanowire $A(AB)_6(ABC)_4A(BA)_6B$. As shown in the lower figures the boundary units consist of hexagons and triangles.

The last example that we give of nanowires with two faults is shown in Fig. 10b. The wire is labeled as $(BA)_6(ABC)_4A(AB)_6$. In this case the boundaries between the fcc and the hcp parts consist of rotated hexagons. The characteristics of these two examples can be found taking the origin at the hexagonal unit in center of the fcc wire.

5. An application: TEM image and electron diffraction simulations of fcc and hcp Co nanowires

As already stated in the introduction, in order to correctly model the properties of nanowires it is of fundamental importance to have a good knowledge of the atomic structure

of this kind of systems. In this respect, transmission electron microscopy (TEM) images and diffraction patterns have been extensively used to analyze both the global and local atomic organization of various types of nanostructures and useful structural information has been obtained.

When performing TEM experiments, electrons coming from the microscope gun are strongly scattered by the crystal potential inside the material. Furthermore, since the image formation is an interference phenomenon, theoretical studies of the properties of the electron wave moving through the structure can be performed.

In this section, we present theoretical simulations of TEM images as well as diffraction patterns of some representative Co nanowires. We consider single crystal (fcc) and polycrystalline nanowires having an average diameter of 15 Å and different wire lengths, in the range of 28–41 Å. The properties of the incident electron wave moving through a given structure are obtained under the assumption of elastic scattering theory, and by using the multi-slice method (based on the physical optics approach) as implemented in the simulaTEM software developed by Gómez and Beltrán [10]. This software provides a direct solution of the integral equivalent of the time independent Schrödinger equation, used in scattering theory. The calculations were made simulating a JEOL 4000 microscope with a defocus condition of -405.5 Å.

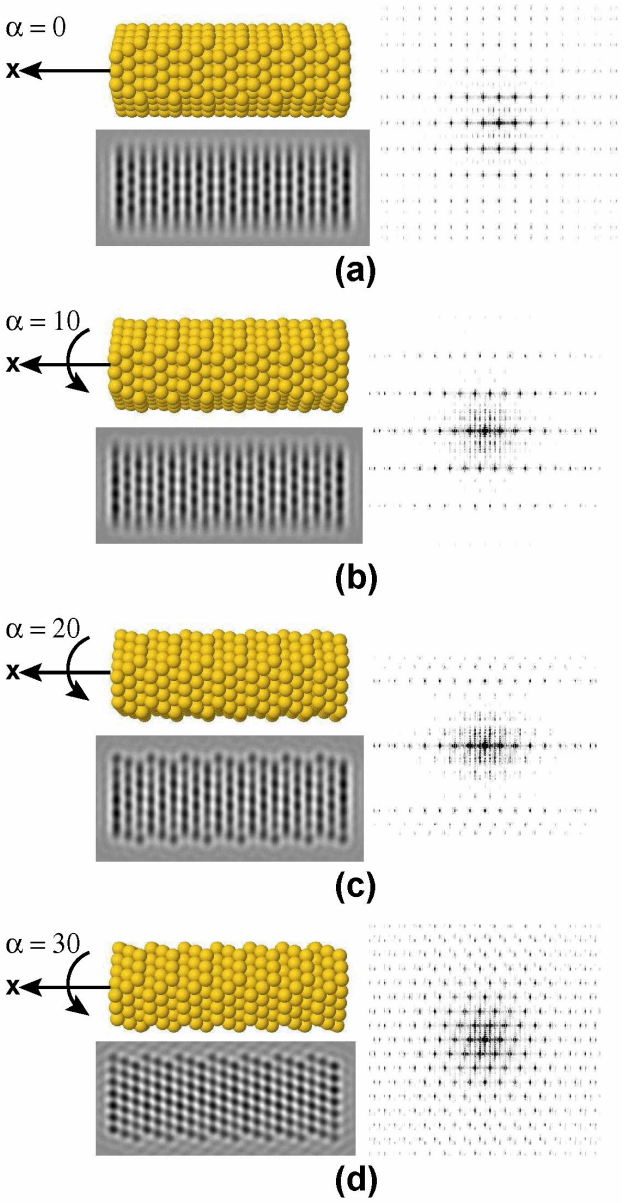

FIGURE 11. A fcc nanowire with 763 atoms. In each panel we show the hard ball model, the TEM image and the electron diffraction pattern. (a) Original wire, (b) rotated by 10°, (c) rotated by 20°, and (d) rotated by 30°.

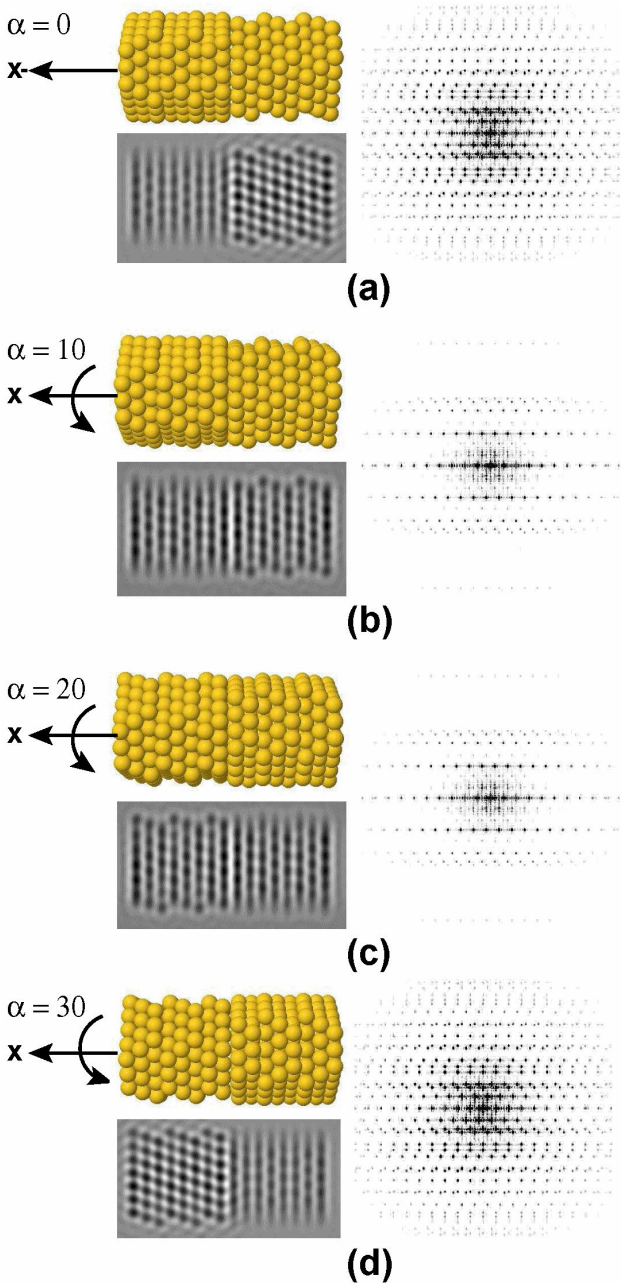

FIGURE 12. Same as Fig. 11 for a faulted fcc wire structure with the right segment rotated 30^0.

In Figs. 11 to 13, we show the hard-ball models of our considered structures, as well as the corresponding simulated TEM images and the diffraction patterns (DP). Calculations have been performed for different relative orientations between the incident beam and the axis of the structures. In fact, by starting with the cobalt nanowires shown in Figs. 11a, 12a, and 13a we perform three rotations of 10, 20, and 30° around the x-axis (as shown in the figures) to obtain different surface orientations as observed from Figs. 11b–11d, 12b–12d, and 13b–13d, respectively. In all the figures we can clearly appreciate that, when the orientation of the surface is changed with respect to the incident beam, strong variations in the contrast of the TEM images are found. This is particularly the case when going from the systems shown in Figs. 12a to 12d where the two fcc grains forming the wire are clearly visible. However, when they are rotated by $\alpha = 10$ their coexistance is more difficult to appreciate. We must comment that, for our considered defocus condition (-405.5 Å), well defined black spots correspond to high linear densities of Co atoms located perpendicular to the plane of the figures. Actually, the variations (reductions) in these linear densities of atoms that occur (in the plane of the figure) when the wires are rotated around the x-axis are the origin of the appearance of diffuse (light-gray) areas, as can be clearly seen in the surface of the wires (see Figs. 11a and 11b, as well as in Figs. 13a and 13b).

Interestingly, we notice from Fig. 12 (where we consider a polycrystalline structure made of two fcc grains attached to each other with a different relative orientation) that the interface between the two fcc volumes (see the hard-ball model

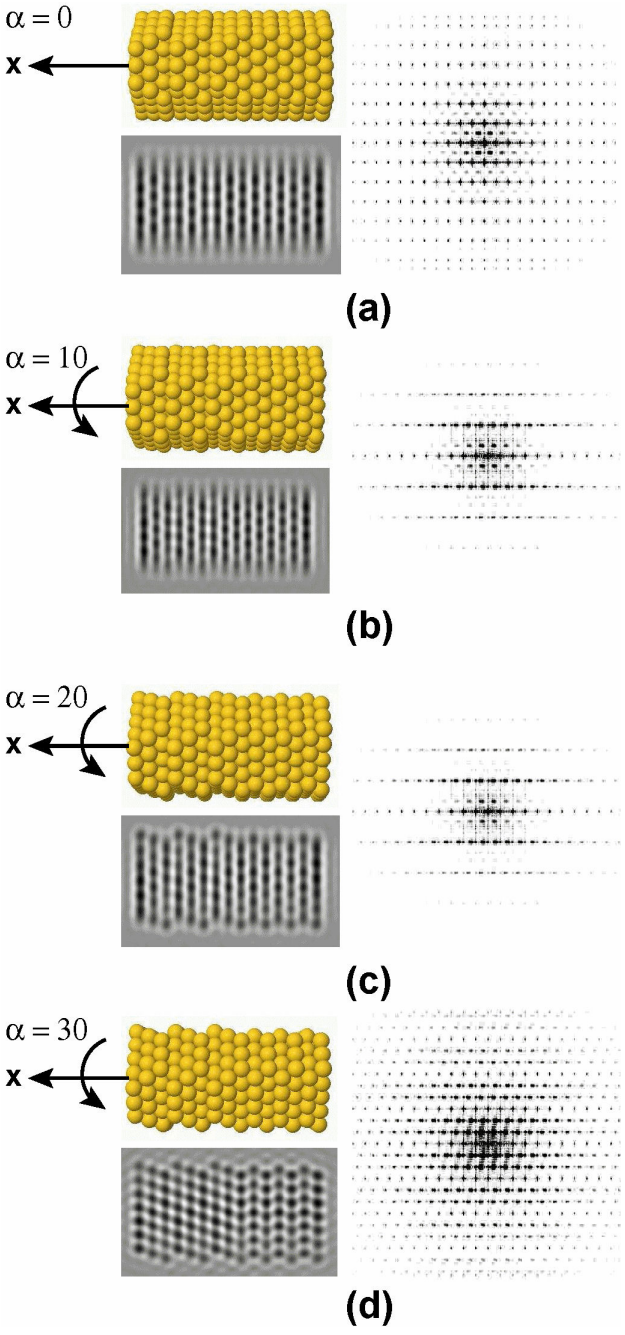

FIGURE 13. Same as Fig. 11 for a faulted fcc-hcp$_z$ nanowire with 546 atoms (see Fig. 8a).

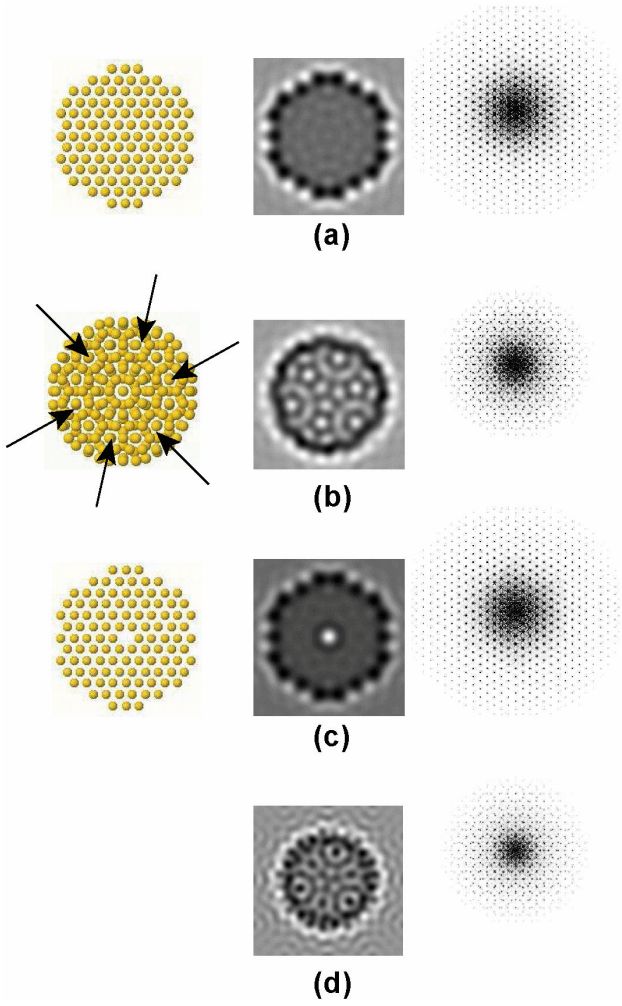

FIGURE 14. The cross section of a) a pure fcc wire, b) the polycrystalline structure shown in Fig. 12, and c) a single crystal fcc wire specified in Fig. 11, but in which we have removed all the atoms located along the principal symmetry axis (x-axis) of the structure.

of the structure) is clearly defined by a more intense white band, and the simulated images can thus provide relevant information not only about the general morphology, but also about the internal structure of our considered Co nanowires.

From Figs. 11–13 we observe also that the simulated diffraction patterns (right column) are also very sensitive to the structure and surface orientation of our considered Co nanostructures. In particular notice from Figs. 11 to 13 that, in contrast to the TEM sequence (where only slight variations in the calculated images are seen), the diffractions patterns are found to be more strongly perturbed when varying the tilting angle α. In general, there is a remarkably large number of spots that are forbidden for small values of α but that later on appear when the tilting angle increases. This fact shows that both types of experimental measurements are complementary imaging techniques that need to be used in order to obtain a more complete structural information of Co nanowires.

We would like to briefly comment also some interesting results related to the analysis of both the TEM images and diffraction patterns (DP) of the cross section of our considered wires. In Figs. 14a and 14b we show, as in previous cases, the hard-ball model for the cross section of a pure fcc wire as well as for the polycrystalline structure shown in Figs. 11 and 12, respectively, together with their corresponding simulated TEM images and calculated diffraction patterns. First, it is important to note that when comparing the diffraction patterns of the single crystal and polycrystalline structures we can clearly appreciate notable differences, reflecting (as in previous cases) the contrasting existing local atomic environments. However, a more interesting situation arises when comparing the calculated TEM images. From Fig. 14a we observe that the single crystal fcc nanowire is characterized by the presence of a transversal dark-gray region having no interesting features. In contrast, in the polycrystalline structure shown in Fig. 14b we note the appearance of well defined white (transparent) areas which are symmetrically located around the cross section of the wire. Actually, by looking at the hard-ball model of this structure we see that the polycrystalline wire is indeed defined as a channel-like atomic array, and that the white areas of the TEM image are located exactly in the same position than some of the channels existing in the wire (marked by arrows). It is important to remark from Fig. 14b that the previous channels are not empty, however; we have found that the Co atomic columns located in the central region of these cavities are not revealed in the calculated spectra. As a consequence, in this case, the image does not reveal in general all the structural features of the wire.

Actually, it is interesting to compare the results shown in Fig. 14b with the TEM and diffraction patterns shown in Fig. 14c, which correspond to the single crystal fcc wire specified in Fig. 11, but in which we have removed all the atoms located along the principal symmetry axis (x-axis) of the structure. From the figure we can appreciate that the missing atoms define an atomic-sized hollow cavity in the central region of the wire that is reflected, in the calculated TEM image also as a white (transparent) circular region, being similar to those obtained in Fig. 14b. In this respect, we have found that this apparent misleading result can be easily understood by varying the defocus condition in our simulations. In fact, if we consider a value for the defocus of -255.0 Å and recalculate the TEM and diffraction patterns of Fig. 14b we obtain a significantly different transmission electron microscopy image shown in Fig. 14d, in which well defined black spots now appear in the central region of the cavities. These spectral features clearly reveal the presence of the linear arrays of Co chains present in the wires as observed from hard ball model shown in Fig. 14b, and underline also the crucial role played by the microscope parameters in the complete structural characterization of these kind of nanostructures.

6. Summary and conclusions

In this work, we have presented the geometrical characterization of nanowires grown in different directions and with various crystallographic structures and lengths. We have addressed wires with single fcc and hcp structures grown along the (111) and z axis directions, respectively. Furthermore since stacking faults are well known to occur in these kind of systems, we have additionally considered wires with one and two growing defects. To help people interested in calculating physicochemical properties of these nanostructures, and in order to exploit the symmetry of the system, we have identified the number of equivalent sites depending on the particular geometry and dimension of the system. We have provided complete tables that can be consulted and used as starting points for theoretical studies.

We have also simulated the TEM images and electron diffraction patterns of some representative pure and stacked fcc-hcp wires. Our results show that, although notable differences between most of the cases are observed, it is clear that in order to well characterize a given structure it is necessary to obtain a detailed tilting sequence of TEM images. Furthermore, we have observed that the defocus parameter plays an important role in the contrast of the calculated images and that, in some cases, the simulated data do not necessarily reflect a well defined structural features. Finally, we conclude that structural analysis based only in TEM images may not be conclusive and additional experimental characterization needs to be performed.

Acknowledgements

The authors would like acknowledge the financial support from CONACyT (México) through grants No. 45928-L (R.A.G.-L.), No. 50650 (R.A.G.-L. and J.M.M.-C.), No. 61489 (J.L.R.-L.), and No. 61417 (J.L.M.-L); partial finantial support from PIFI (México) through grant 2007-24-21. Computer resources from the Centro Nacional de Supercómputo (CNS) from the Instituto Potosino de Investigación Científica y Tecnológica (IPICyT), San Luis Potosí, México, are also acknowledged.

1. F. Rosei, *J. Phys.: Condens. Mater.* **16** (2004) S1371; K. Ostrikov, *Rev. Mod. Phys.* **77** (2005) 489; I. Denysenko and K. Ostrikov, *Appl. Phys. Lett.* **90** (2007) 251501; M. Keidar, Y. Raitses, A. Knapp, and A.W. Wass, *Carbon* **44** (2006) 1022; M. Xu, S. Xu, J.W. Chai, J.D. Long, and Y.C. Ee, *Appl. Phys. Lett.* **89** (2006) 251906; Uroŝ Cvelbar, K. Ostrikov, A. Drenik, and M. Mozetic, *Appl. Phys. Lett.* **92** (2008) 133501.
2. J.L. Martín, J. Nogués, K. Lui, J.L. Vicent, and I.K. Schuller, *J. Mag. Mag. Mat.* **256** (2003) 449.
3. C. Chappeti, A. Fert, and F. Nguyen Van Dau, *Nature Mater. Insight* **6** (2007) 813; M. Hayashi, L. Thomas, R. Moriya, C. Rettner, and S. Parkin, *Science* **320** (2008) 209; S.P. Parkin, M. Hayashi, and L. Thomas, *Science* **320** (2008) 190.
4. T. Thurn-Albrecht *et al.*, *Science* **290** (2000) 2126.
5. R.R. Schlittler *et al.*, *Science* **292** (2001) 1136.
6. F. López-Urías *et al.*, *Phys. Rev. Lett.* **94** (2005). 216102
7. M. Brands, B. Leven, and G. Dumpich, *J. Appl. Phys.* **97** (2005) 114311.
8. R.A. Guirado-López, J.M. Montejano-Carrizales, and J.L. Morán-López, *Phys. Rev. B* **77** (2008) 134431.
9. A. Kazadi Mukenga Bantu, J. Rivas, G. Zaragoza, M.A. López-Quintela, and M.C. Blanco, *J. Applied Phys.* **89** (2001) 3393; Takeshi Fujita, Yasuhito Hayashi, Tomoharu Tokunaga, and Kazuo Yamamoto, *Applied Phys. Lett.* **88** (2006) 243118; G.J. Strijkers, J.H.J. Dalderop, M.A.A. Broeksteeg, H.J.M. Swagten, and W.J.M. de Jonge, *J. Applied Phys.* **86** (1999) 5141; K. Ounadjela *et al.*, *J. Appl. Phys.* **81** (1997) 5455; R. Ferré, K. Ounadjela, J.M. George, L. Piraux, and S. Dubois, *Phys. Rev. B* **56** (1997) 14066; E. Snoeck *et al.*, *Appl. Phys. Lett.* **82** (2003) 88; J.M. García *et al.*.
10. The SimulaTEM program was developed by A. Gómez Rodríguez and L.M. Beltrán del Río, IF-UNAM (2007).